Measurement of Developing Turbulent Flows in a 90-Degree Square Bend with Spanwise Rotation

Young Don Choi*
Professor, Department of Mechanical Engineering, Korea University, Sungpukku, Seoul 136-701, Korea
Dong Chul Kim
Graduate School, Department of Mechanical Engineering, Korea University, Sungpukku, Seoul 136-701, Korea
Kun Hee Lee
Associate Professor, Department of Mechanical Engineering, Wonkwang University, Iksan, Chunbuk 570-749, Korea

Mean flow and turbulence properties of developing turbulent flows in a 90 degree square bend with span-wise rotation are measured by a hot-wire anemometer. A slanted wire is rotated into 6 orientations and the voltage outputs from them are combined to obtain the mean velocity and the Reynolds stress components. Combined effects of the centrifugal and Coriolis forces due to the curvature and the rotation of the bend on the mean motion and turbulence structures are investigated experimentally. Results show that the two body forces can either enhance or counteract each other depending on the flow direction in the bend.

Key Words : Rotating Curved Duct, Hot-wire measurement, Reynolds Stress, Coriolis Force, Turbulent Flow

Nomenclature

C_P : Pressure coefficient
$\overline{C_P}$: Mean pressure coefficient
D_H : Hydraulic diameter of duct
D_n : Dean number $=\mathrm{Re}(D_H/R_C)^{1/2}$
E : Instantaneous voltage of hot-wire
e : Fluctuating voltage of hot-wire
e_r : Radial direction unit vector
$\boldsymbol{F_C}$: Coriolis force vector
F_r : Resultant force
$\boldsymbol{F_r}$: Resultant force vector
$\boldsymbol{F_R}$: Centrifugal force vector associated with the rotation of bend
F_C : Centrifugal force associated with bend rotation
k_{θ_i} : Coefficient of hot-wire orientatation
$K_{E_iE_j}$: Covariance between wires i and j
K_S : Coefficient of hot-wire characteristics
P : Pressure
$\boldsymbol{R}$: Radius vector from the axis of rotation
R : Radius from the axis of rotation
R_C : Radius of duct curvature
$\mathrm{R_C}$: Rotation number $(=\Omega r_m/W_B)$
Re : Reynolds number $(=W_B D_H/v)$
$\mathrm{R_o}$: Rossy number $(=\Omega D_H/W_B)$
r_m : Mean radius of duct curvature
U : Normal mean velocity component
U_e : Effective velocity
$\overline{u_i u_j}$: Reynolds stress tensor
V : Radial mean velocity component
v : Radial fluctuating velocity
V_λ : Resultant velocity vector
W : Stream-wise velocity component
W_B : Stream-wise bulk velocity

* Corresponding Author,
E-mail : ydchoi@korea.ac.kr
TEL : +82-2-3290-3325; **FAX** : +82-2-928-1067
Professor, Department of Mechanical Engineering, Korea University, Sungpukku, Seoul 136-701, Korea.
(Manuscript **Received** December 7, 2004; **Revised** April 6, 2005)

w : Stream-wise fluctuating velocity
$\overline{X_\theta}$: Mean effective velocity
X : Normal coordinate
$\tilde{X}_\theta$: Effective velocity
Y : Radial coordinate
Z : Stream-wise coordinate
$\gamma_{E_i E_j}$: Correlation coefficient between cooling velocities of adjacent wire orientations
θ : Rotation angle of hot-wire, bend angle from entrance
κ : Experimental constant
ν : Kinetic viscosity
ξ : Angle between V_λ and a wire
ρ : Density
σ^2 : Variance of a given quantity
Ω : Angular velocity
φ : Angle between Coriolis and centrifugal forces associated with bend rotation

Subscripts

l, m : Dummy indices which take the valves 1 to 3
1, 2, 3, 4, 5, 6 : Refers to the six probe measuring positions
θ : Rotation angle of hot-wire, bend angle

1. Introduction

Information on the turbulent flows in rotating, curved ducts are of great importance, for instance, in the design of rotating devices such as turbines, pumps and compressors. In such flows, the Coriolis and centrifugal forces arising from the imposed system rotation and bend curvature may act both on the mean motion and turbulence structures. Consequently, the reacting forces on the mean motion may encounter rapid changes in direction and magnitude with the progress of flow along the bend. If the two body forces are confluent, the resultant force may enhance the generation of secondary flows whereas if the forces counteract, they may decrease the secondary flows. It is highly desirable to decouple the contributions of the body forces on the mean motion and turbulence structures. However it is not easy to isolate their individual contribution in the rotating bend flows in practice.

There have been extensive studies on the effects of Coriolis and centrifugal forces in rotating plane channel flows. They include the large eddy simulations by Kim (1983), and Tafti and Vanka (1991), experimental study by Koyama and Ohuchi (1985), the direct numerical simulation by Kristofferson and Anderson (1990), and the application of second-moment closure by Launder et al.(1987), and Launder and Tselepidakis (1994).

The curvature and system rotation of a bend can destabilize or stabilize the flow in some regions. The mechanism for this destabilizing and stabilizing phenomena have been examined extensively in plane channel flows rotating in orthogonal mode, by Johnston (1972), Launder et al.(1989), Launder and Tselepidakis (1994), Kristoffersen and Anderson (1993), Anderson and Kristofferson (1995), and Patterson and Anderson (1997). A comprehensive review of the literature on heat transfer in rotating plane channels was provided by Morris (1981), Kajishima et al.(1991), and Murata and Mochizukv (1999). Kajishima et al.(1991), Murata and Mochizuki (1999) performed large eddy simulations to examine the effects of the Coriolis force on turbulent heat transfer characteristics in the curved channel flows rotating in orthogonal mode. Second moment closures were employed by Bo et al. (1995) and Younis (1993) to predict the turbulent heat transfer in orthogonally rotating square duct flows.

Development of turbulence models applicable to rotating curved duct flows has been difficult due to the lack of experimental data for mean velocity and Reynolds stress distributions. The turbulent flow in a rotating 90° bend with a square cross-section has several qualities that make it well suited for a benchmark test flow to develop the second moment closures. The effects of Coriolis and centrifugal forces on the mean motion and turbulence structures can easily be decoupled, due to the simple shape of the flow passage.

The flow configuration of this study is the 90-degree rotating bend of a square cross-section followed by a straight duct section. The objective of the present study is to make detailed measurements, using a hot-wire anemometry technique, of the developing turbulent flow in the 90-degree *rotating square bend and upstream tangent in* order to investigate the combinative effects of rotation and curvature of bend on the mean motion and turbulence structures.

Figure 1 shows a schematic diagram of the rotating 90-degree bend and defines the coordinate system and symbols used. The radius of the curvature to hydraulic diameter ratio (Rc/D_H) of the bend is 3.375, and the bend angle is 90 degrees. X and Y map the cross-sectional plane, while progress around the bend is expressed through angle θ. In this rotating bend flow, 3 kinds of body forces, acting on a fluid particle, affect both on the mean motion and turbulence structures. They are:

The centrifugal force associated with the curvature of bend

$$F_{C,C}=\rho\frac{W^2}{r} \tag{1}$$

The centrifugal force associated with the rotation of bend

$$\boldsymbol{F}_R=-\rho\boldsymbol{R}\times\Omega\times\Omega \tag{2}$$

The Coriolis force associated with the rotation of bend

$$\boldsymbol{F}_C=-2\rho\Omega\times V$$

Normalizing by $\rho W_B^2/r_m$ the radial components of the resultant force of the three forces along the centerline of the bend yields

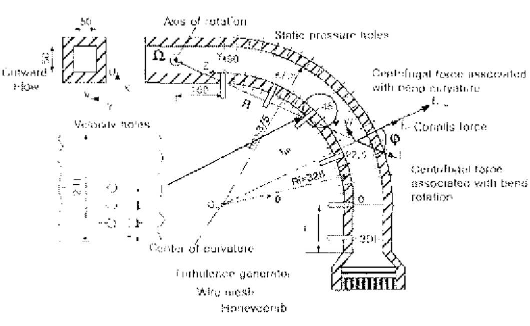

Fig. 1 Schematic diagram showing the bend and tangents, the two coordinate systems and the three velocity components

$$\frac{\boldsymbol{F}\cdot\boldsymbol{e}_r}{\rho W_B^2/r_m}=\frac{F_r}{\rho W_B^2/r_m} \tag{3}$$
$$=1+2\mathrm{R_C}+\frac{R\cos\varphi}{r_m}\mathrm{R_C^2}$$

where $\mathrm{R_C}$ is the rotation number defined as $\frac{\Omega r_m}{W_B}$

Equation (3) shows that the rotation number $\mathrm{R_C}$ is the primary parameter that determines the characteristics of rotating flow in a curved duct.

In the rotating plane channel flows, the Rossby number $(\mathrm{R_o}=\Omega D_H/W_B)$ has been used as a primary parameter that describes the rotating flow characteristics (Johnston et al. (1970)). In a rotating bend flow of a square cross-section, however, it should be replaced by rotation number $\mathrm{R_C}=\Omega r_m/W_B(=R_o r_m/D_H)$, the ratio of the Coriolis to the centrifugal forces along the centerline of the bend, where r_m is the mean curvature radius of the bend.

Two kinds of flow modes are studied experimentally in this study. One is the outward flow mode in which the flow is blown out from the center hole toward outward direction. In this flow mode, the Coriolis and centrifugal forces combine in a destructive way to decrease the secondary flow intensity. On the other hand, in the inward flow mode, in which the flow is suctioned through the test section toward center hole that is located at the rotating hollow shaft, the Coriolis force is combined with the centrifugal force to promote the secondary flow. The data obtained by the present experiment will be used in many ways for developing and testing comprehensive three dimensional turbulence models.

2. Experiment

2.1 Experimental apparatus

The basic components of the experimental apparatus are shown schematically in Figs. 2 and 3. It is comprised of a test section, a 90-degree bend with a 50 mm square cross-section, a rotating disc of 1.92 m diameter, an Ag-Ni precision slip ring constructed to transmit the signal from the rotating test section to the stationary anemometer, an electric power supply for the automatic traversing mechanism, a variable speed motor, a speed reduction gear mechanism, centrifugal blower, an orifice flowmeter, and a hot-wire anemometer system. The lengths of the inlet and outlet tangents of the bend are 1 and 2.223 hydraulic diameters, respectively. The section is constructed from an 8 mm thickness acryl sheet providing rigid, transparent walls. Honeycomb and wire mesh screens are installed upstream of the test section to eliminate the secondary motion and the turbulence involved in the intake flow. Down-

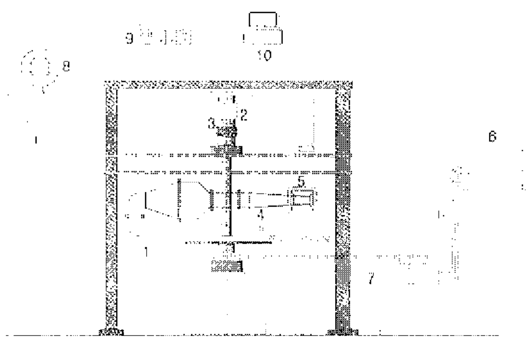

1. Rotating disc
2. Slip-ring for hot-wire anemometer and traversing mechanism
3. Slip-ring for AC power
4. Traversing mechanism
5. Test section
6. Variable motor
7. Speed reducer
8. Blower
9. Hot-wire anemometer
10. Personal computer

Fig. 2 Schematic diagram of experimental apparatus

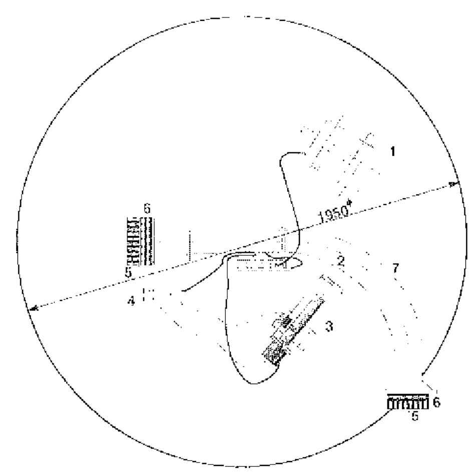

1. Controlling computer
2. Rotating probe
3. Automatic traversing mechanism
4. Control box
5. Setting chamber
6. Turbulence generator
7. Test section

Fig. 3 Plan view of rotating disc

stream of the wire mesh, a turbulence generator, which consists of a 4 mm diameter tube bank with a 10 mm pitch, is installed to generate uniform inlet turbulence. The speed of the rotating disc is controlled by a variable speed motor and a bevel gear speed reduction mechanism. The hot wire probe is traversed by an automatic mechanism, which is installed on the rotating disc. Translation tolerance of the automatic traversing mechanism is 1/200 mm and the rotation tolerance is 1/2 degree. Air flow through the test section is provided by a centrifugal blower, and the flow rate is measured by a $D-\frac{1}{2}D$ orifice flowmeter. Intake air temperature of the test section rises slowly due to the heat generation of the blower and reaches a steady state at about 1 hour of operation.

As shown in Fig. 1, static pressure holes are installed on the inner and outer walls along the symmetric plane of the bend at every five degree increment. The pressure holes are connected to a pressure transducer by a polyvinyl tube to the pressure scanning box. Velocity holes are installed at 7 stations: $0.5D_H$, $-0.D_H$, $0°$, $22.5°$, $45°$, $67.5°$ and $90°$ on the outside wall. At each station, 4 velocity holes are located at the positions where $\frac{2X}{D}=0.25, 0.5, 0.75, 1.0$.

The 3-dimensional velocity and 6 Reynolds stress components were calculated by the correlations which combine the mean and fluctuating voltages measured by S and I types hot-wire probes.

2.2 Measurement of mean velocity components

Rotating the S-type hot-wire θ degree from the reference position, which is inclined 45° from the Y-Z plane as shown in Fig. 4, the coordinate of point A would be $\left(-\frac{1}{2}\cos 45° \sin\theta,\ -\frac{1}{2}\cos 45°,\ -\frac{1}{2}\cos 45° \cos\theta\right)$.

Denoting the resultant velocity vector by

$$V_A = U\mathbf{i} + V\mathbf{j} + W\mathbf{k} \tag{4}$$

the angle ξ between resultant velocity vector V_A and position vector A can be obtained by the dot product of the two vectors as follows:

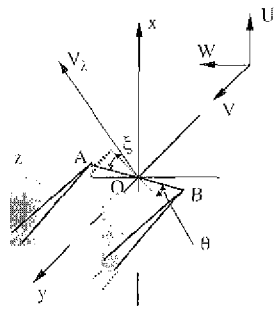

Fig. 4 Schematic diagram showing a S type wire probe rotated θ degree from reference position

$$\xi=\cos^{-1}\left(\frac{W\cos\theta-V-U\sin\theta}{\sqrt{2}\,V_\lambda}\right) \tag{5}$$

where V_λ is the magnitude of the resultant velocity. If a linearized hot wire anemometer system is used, then the measured instantaneous voltage is related to the effective velocity (U_e):

$$E_\theta=K_S U_{e\theta} \tag{6}$$

where K_S is a proportionality constant and the subscript θ denotes the rotated angle of the probe from the reference position. Champagne (1967) suggested a relation between effective and resultant velocities,

$$U_{e\theta}=V_\lambda(\sin^2\xi+\kappa^2\cos^2\xi)^{\frac{1}{2}} \tag{7}$$

where k is an empirical constant. In the present study, $\kappa=0.2$ was adopted. Substituting equations (5) and (7) into (6), one may arrive at

$$\begin{aligned}E_\theta=\frac{K_s}{\sqrt{2}}[&U^2(2-\sin^2\theta+\kappa^2\sin^2\theta)+(1+\kappa^2)V^2\\&+W^2(2-\cos^2\theta+\kappa^2\cos^2\theta)+2VW(1-\kappa^2)\\&+2UW\cos\theta\sin\theta(1-\kappa^2)-2UV\sin\theta(1-\kappa^2)]^{\frac{1}{2}}\end{aligned} \tag{8}$$

Replacing the instantaneous values of E_θ, U, V, and W in Eq. (8) by their mean and fluctuating components, and expanding them in a Taylor series (neglecting terms of order higher than fifth), the following fourth order equation for the mean effective velocity $\overline{X_\theta}$ is obtained (Choi et al.(1990)):

$$3\overline{X_\theta}^4-8\overline{E_\theta}\,\overline{X_\theta}^3+6(\overline{E_\theta}^2+\overline{e_\theta}^2)\overline{X_\theta}^3-\delta_\theta=0 \tag{9}$$

where

$$\overline{X_\theta}'=\frac{K_S\overline{X_\theta}}{\sqrt{2}} \tag{10}$$

$$\delta_\theta=\overline{E_\theta}^4+6\overline{e_\theta^2}\,\overline{E_\theta}^2+4\overline{e_\theta^3}\,\overline{E_\theta}+\overline{e_\theta^4} \tag{11}$$

where

$$\begin{aligned}\overline{X}_\theta=(&k_{\theta1}\overline{U}^2+k_{\theta2}\overline{V}^2+k_{\theta3}\overline{W}^2+k_{\theta4}\overline{V}\,\overline{W}\\&+k_{\theta4}\overline{U}\,\overline{W}+k_{\theta4}\overline{U}\,\overline{V})^{1/2}\end{aligned}$$

$$k_{\theta1}=2-\sin^2\theta+\kappa^2\sin^2\theta$$

$$k_{\theta2}=1+\kappa^2$$

$$k_{\theta3}=2-\cos^2\theta+\kappa^2\cos^2\theta$$

$$k_{\theta4}=2(1-\kappa^2)$$

$$k_{\theta5}=2\cos\sin\theta(1-\kappa^2)$$

$$k_{\theta6}=2\sin\theta(1-\kappa^2)$$

If $\overline{E_\theta}$, $\overline{e_\theta^2}$, $\overline{e_\theta^3}$, $\overline{e_\theta^4}$ are measured for each probe angle, $\overline{X_\theta}$ can be calculated from Eq. (9) by rotating the S-type probe into $\theta=60°$, $90°$, $120°$ and $270°$, and followed by the I-type probe into $60°$, $120°$. $\overline{E_\theta}$, $\overline{e_\theta^2}$, $\overline{e_\theta^2}$, $\overline{e_\theta^2}$ were measured for each angle. If the positive roots of equation (9) for the corresponding probe angles are denoted by X_1'', X_2'', X_3'', X_4'', X_5'', and X_6'', many sets of simultaneous equations for $\overline{U}$, $\overline{V}$, and $\overline{W}$ can be obtained from equation (8). Among the sets of equations, we can choose the optimal relation that can give minimum uncertainty of the mean velocity calculation due to its diagonal dominance of the solution matrix. The resulting relations are written as

$$U=[(\overline{X_5''})^2-(\overline{X_6''})^2]/[\sqrt{3}K_S^2(1-\kappa^2)\overline{W}] \tag{12}$$

$$\begin{aligned}\overline{V}=[&2(\overline{X_1''})^2-2(\overline{X_2''})^2-(\overline{X_5''})^2+(\overline{X_6''})^2]\\&/[2K_S^2(1-\kappa^2)\overline{W}]\end{aligned} \tag{13}$$

$$\overline{W}=[(\overline{X_3''})^2+(\overline{X_4''})^2-(1+\kappa^2)(\overline{U}^2+\overline{V}^2)]^{\frac{1}{2}} \tag{14}$$

2.3 Measurement of reynolds stress components

In the present study, the Janjua et al's.(1982) correlation was used to calculate the Reynolds stress components. The tensor form for the correlation is

$$\overline{u_l u_m}=\sum_{i=1}^{6}\frac{\partial\overline{U_l}}{\partial\overline{E_i}}\frac{\partial\overline{U_m}}{\partial\overline{E_i}}\overline{\sigma^2_{E_i}}+\sum_{i=1}^{6}\sum_{i\neq j, j=1}^{6}\frac{\partial\overline{U_l}}{\partial\overline{E_i}}\frac{\partial\overline{U_m}}{\partial\overline{E_j}}\overline{K_{E_iE_j}}$$
$$-\left[\frac{1}{2}\sum_{i=1}^{6}\frac{\partial^2 U_l}{\partial\overline{E_i^2}}\overline{\sigma^2_{E_i}}+\sum_{i=1}^{6}\sum_{i<j, j=1}^{6}\frac{\partial^2\overline{U}}{\partial\overline{E_i}\partial\overline{E_j}}\overline{K_{E_iE_j}}\right]$$
$$\times\left[\frac{1}{2}\sum_{i=1}^{6}\frac{\partial^2 U_m}{\partial\overline{E_i^2}}\overline{\sigma^2_{E_i}}+\sum_{i=1}^{6}\sum_{i<j, j=1}^{6}\frac{\partial^2\overline{U_m}}{\partial\overline{E_i}\partial\overline{E_j}}\overline{K_{E_iE_j}}\right] \quad (15)$$

where $\overline{\sigma^2}_{E_i}$ represents $\overline{\sigma^2}_\theta$ for a given probe angle and $K_{E_iE_j}$, is the covariance between wire i and wire j.

Jackson and Lilley (1983) used the following covariance relation in their experimental work :

$$K_{E_iE_j}=\gamma_{E_iE_j}(\overline{\sigma^2_{E_i}}\,\overline{\sigma^2_{E_j}})^{\frac{1}{2}} \quad (16)$$

where $\gamma_{E_iE_j}$ is the correlation coefficient between wires i and j. King (1978) made a certain assumption by calculating the covariance coefficient. He argued that if two wires are separated by an angle of 30 degrees, the contribution of the correlation coefficient would be related by the cosine of the angle between the wires as follows :

$$\gamma_{E_iE_j}=\cos 30°=0.87 \quad (17)$$

When separation angle θ is a multiple of 30°, he used the following correlation coefficients :

$$\gamma_{E_iE_j}=0.8(\cos 30°)^n \quad (18)$$

Choi et al.(1990) extended King's relation to angles θ, that are not multiples of 30°. Choi's correlation coefficient for separation angle $\theta=30n+\alpha$ is written as

$$\gamma_{E_iE_j}=0.8(\cos 30°)^n\cos\alpha \quad (19)$$

If mean voltage $\overline{E_\theta}$, square mean fluctuating voltage component $\overline{e_\theta^2}$, and cubic mean of fluctuating voltage component $\overline{e_\theta^2}$ are measured for each probe angle, the Reynolds stress correlation Eq. (15) can be calculated by using correlation (19).

2.4 Scope of experimental program and data uncertainty

Various combinations of the present experimental program are tabulated in Table 1.

Uncertainty analysis was performed based on the method suggested by ASME Performance Test Codes (1987). It is assumed that the equipment has been constructed correctly and calibrated properly to eliminate fixed errors. Thus, the uncertainties of the measured quantities in the present experiments are assumed to be random with normal distribution. The uncertainty of the Reynolds number and digital manometer is estimated as 0.94% and 0.2%, and the uncertainties of hot-wire for mean and fluctuating velocities are estimated as 4.4% and 2.9%, respectively. Therefore, the combined uncertainties of pressure coefficients, and mean and fluctuating velocities are estimated as 0.96%, 4.5% and 3.0%, respectively.

Table 1 Various combinations of experimental parameters

Reynolds Number	Rotating speed (rpm)	Rossby number	Rotation number
20,000	0	0.0	0.0
60,000	60	0.0427	0.187
40,000	45	0.0481	0.210
40,000	60	0.0641	0.280
30,000	60	0.0854	0.374
20,000	60	0.1282	0.561
20,000	−60	0.1282	−0.561
20,000	−75	−0.1603	−0.701

3. Results and Discussion

Distributions of pressure coefficients along the inner and outer walls are compared in Fig. 5 for various rotation numbers. The pressure coefficient is defined as

$$C_p=\frac{P-P_r}{\frac{1}{2}\rho W_B^2} \quad (20)$$

where W_B is the bulk velocity, P is the local mean static pressure and P_r is the reference pressure measured on the outer wall at the bend inlet. As the flow enters the bend, the pressure coefficient along the outer wall rises quickly while that of inner wall drops almost as quickly. Beyond the entrance region, both pressure coefficients again decrease slowly. However, as the rotation number of the bend increases, differences between the pressure coefficients of the inner and outer walls also increase. For the inward flow mode, Coriolis forces are added to the centrifugal forces associated with the bend curvature in a productive way in the outward radial direction so that it may increase the difference of the pressure coefficients between the inner and outer walls.

In the stationary bend flow, the pressure coefficient along the inner wall drops slowly in the entrance region, but beyond that region remains nearly constant up to the bend exit. As the rotation number increases, however, it decreases more quickly and shows wavy variations as shown in Fig. 5. These wavy variations of pressure coefficients in the rotating bend flows are presumably caused by the rapid change of secondary flow pattern as with the increase of the rotation number of the bend flow.

Comparison of the measured mean pressure coefficients for the various Reynolds numbers and rotation numbers are shown in Fig. 6. Mean pressure coefficient of the square sectioned bend can be defined as

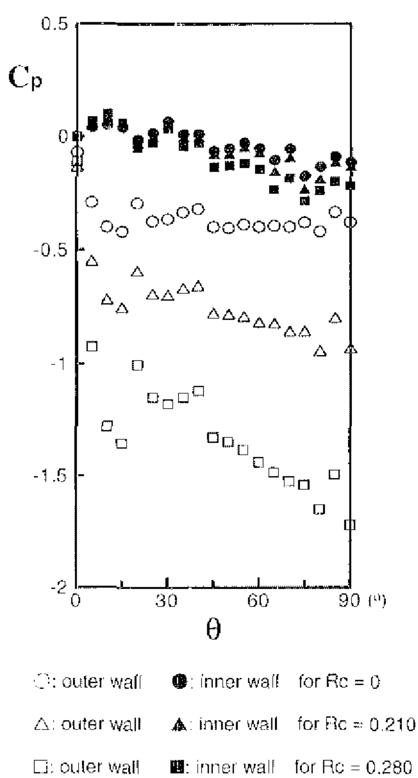

Fig. 5 Comparison of measured pressure coefficients along the inner and outer the walls in the inward flow mode for Re=40,000

$$\overline{C_p}=\frac{(\overline{P}_{inlet}+\overline{P}_{outlet})/2-P_r}{\frac{1}{2}\rho W_B^2} \tag{21}$$

In the stationary duct flow, mean pressure coefficients show significant Reynolds number dependency. However as with the increase of rotation number, the dependency of the Reynolds number disappears while the dependency on the rotation number remains.

It is of interest in Fig. 7 to compare the measured pressure coefficients for the outward flow mode in which the rotation number has negative value. In the outward flow mode, the radial component of the Coriolis force is added to the centrifugal force associated with the bend curvature in a destructive way, thus resulting in a decrease in pressure coefficient differences between the inner and outer walls. Furthermore, *in the entrance region of the bend, the Coriolis* force exceeds the centrifugal force, making the pressure coefficients of the inner wall greater than those of the outer wall. But as the flow progresses around the bend in the outward direction, the trend is reversed. At Rc=−0.561, the reverse of pressure coefficients occurs in the vicinity of

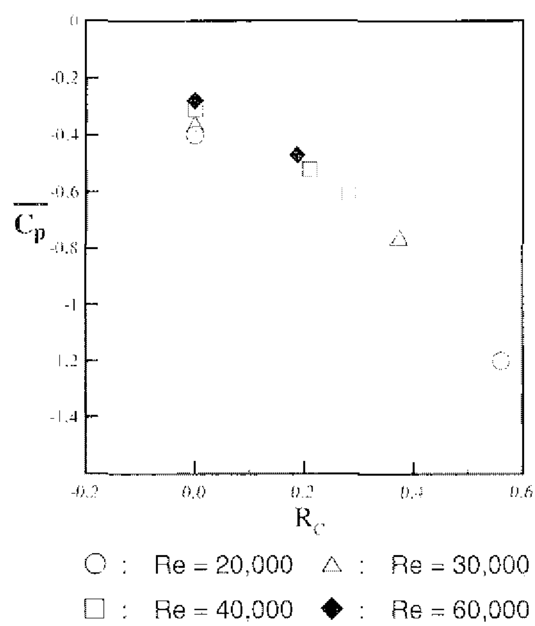

Fig. 6 Variation of mean pressure coefficients with respect to Re

$\theta=30°$ while at Rc$=-0.701$ the reversal point moves to $\theta=55°$. Increase in the Coriolis force in a negative direction as with the decrease of the rotation number may reduce the pressure coefficients of the outer wall so as to move the reversal point in a downward direction.

Figure 8 shows the comparison of the longitudinal variation of measured mean stream-wise and radial velocity profiles of the rotating and stationary bend flows for the inward flow mode. The open symbol indicates the normalized mean velocity components of the stationary bend flow while the solid symbol indicates those of the rotating bend. As the flow progresses along the bend, the location of the maximum mean stream-wise velocity shifts toward the outer wall both in the stationary and the rotating bend flows. In this type of inward flow mode, the rotation of the bend combines the Coriolis and centrifugal forces in a productive way in a radial outward direction, increasing the secondary flow intensity, and thereby promoting the shift of the location of the maximum mean stream-wise velocity toward the outer wall in the entrance region of the bend. However, in the rotating flow, the shifting of the location of the maximum velocity stops after the progress of the 45° flow into the bend. Generally, it is known that a pair of large counter-rotating Eckman vortices appear and grow in the entrance region of the bend and increase up to $\theta=90°$, but after they reach $\theta=90°$, the Eckman vortex pair breaks down into a multi-cell pattern and Dean vortices appear in the outer wall region. Choi et al.(1997) analyzed numerically the developing turbulent flow in the coiled bend of a square cross-section by employing a second moment turbulence closure. In the computation, they captured the occurrence of three pairs of Dean vortices in the outer wall region at around $\theta=180°$ station of the bend. However in the rotating bend flow, the Coriolis and centrifugal forces associated with the bend rotation may affect the mean motion and turbulence structures in a complex manner so that they may include the earlier appearance of Dean vortex pair.

Figure 9 shows the development of normalized mean stream-wise and radial velocity profiles

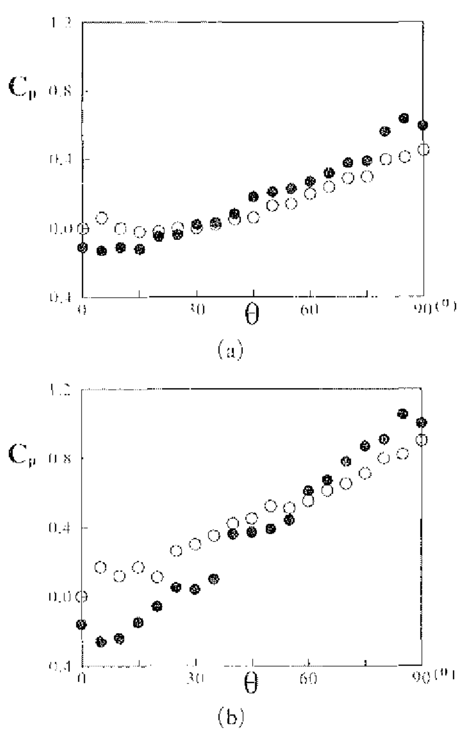

○ :outer wall ● : inner wall

Fig. 7 Comparison of measured pressure coefficients in the outward flow mode for Re=20,000, and (a) Rc$=-0.561$, (b) Rc$=-0.701$

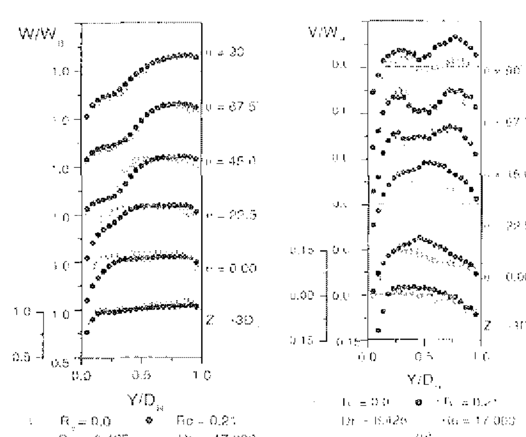

(a) (b)

Fig. 8 Longitudinal variation of measured normalized mean stream-wise velocity (W/W_B) and radial velocity (V/W_B) along the center symmetry plane for the inward flow mode for higher Dean and lower rotation numbers along the symmetry plane for higher rotation number and lower Dean number compared to those shown in Fig. 8. The effect of the decrease in Dean number may exceed the effect of the increase in rotation number, suppressing the mean radial velocity in the bend. However in the upstream tangent, where there is no curvature effect, the increase in rotation number induce the large increase in secondary flow intensity.

In Fig. 10, the variations of measured stream-wise mean velocity profiles of the rotating bend flows for relatively higher Dean and rotation numbers are compared with those of stationary bend flow. In the relatively higher Dean and rotation number flow, as the flow enters the bend from the straight inlet tangent, it is subjected to an abrupt favorable pressure gradient along the inner wall while an adverse pressure gradient along the outer wall. This difference of pressure gradient between the inner and outer wall in the entrance region of the bend may accelerate the flow along the inner wall and decelerate the flow along the outer wall. However, as the flow progresses along the bend, the secondary flow induced by the imbalance of the body forces and pressure gradients may shift the location of the maximum mean stream-wise velocity toward the outer wall both in the stationary and the rotating bend flows. Up to $\theta=45°$, the rotation of the bend promotes the shift of the location of the maximum mean stream-wise velocity toward the outer wall. However, beyond $\theta=45°$, the shifting of the location of the maximum mean stream-wise velocity of the rotating bend flow stops earlier than that of the stationary bend so that it yields a significant decrease of the mean stream-wise velocity profile in the outer wall region. Lee (1992), in the calculation of a rotating 90-degree square sectioned bend flow in the same condition as in that of Fig. 10, found that the bend rotation may advance the occurrence of a large Dean vortex pair up to $\theta=45°$. A Dean vortex pair appearing in the outer wall region of the rotating bend near the symmetry plane beyond $\theta=45°$ may prevent a further shift of the location of the maximum stream-wise velocity toward the outer wall, yielding an obvious decrease of the mean stream-wise velocity in the outer wall region as shown in Fig. 10.

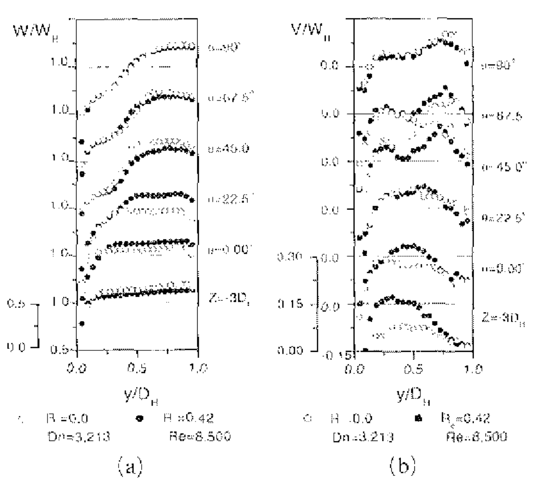

Fig. 9 Longitudinal variation of measured normalized mean stream-wise velocity (W/W_B) and radial velocity (V/W_B) along the symmetry plane in the outward flow mode for lower Dean number and higher rotation number

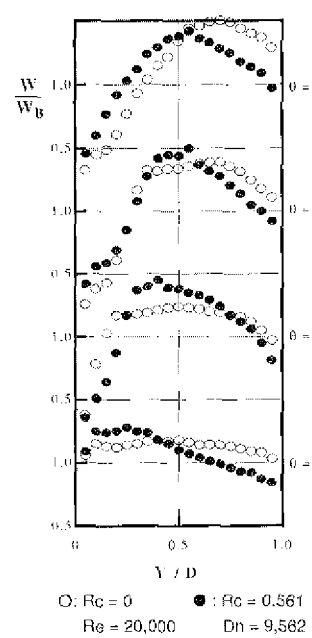

Fig. 10 Longitudinal variation of measured normalized mean stream-wise velocity profiles along the symmetry plane in the inward flow mode for higher Dean and rotation numbers

The decreases in the level of stream-wise and radial rms turbulent velocities and Reynolds shear stress normalized by W_B and W_B^2 are found in Fig. 11 near the suction side in the rotating bend flow. Launder and Tselepidakis (1994) applied a second moment closure to the rotating plane channel flow and computationally validated the indirect effects of the Coriolis generation in the $\overline{vw}$ equation on the level of turbulent kinetic energy and mean square turbulent velocities.

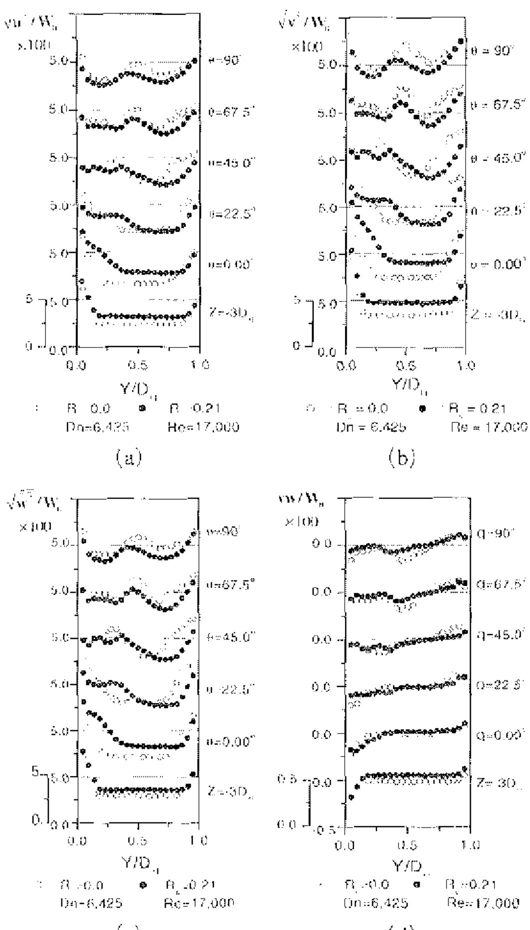

Fig. 11 Longitudinal variation of measured rms turbulent velocities ($\sqrt{\overline{u^2}}/W_B$, $\sqrt{\overline{v^2}}/W_B$, $\sqrt{\overline{w^2}}/W_B$) and Reynolds shear stress ($\overline{vw}/W_B^2$) normalized by W_B and W_B^2 in the inward flow mode for higher Dean number and lower rotation number

In the cylindrical polar coordinates rotating at angular velocity Ω, generation terms of the mean square stream-wise and radial turbulent velocities ($\overline{w^2}$, $\overline{v^2}$) and Reynolds shear stress ($\overline{vw}$) may be written as:

$$P_{\overline{w^2}} = \underbrace{-2\overline{uw}\frac{\partial W}{\partial x} - 2\overline{vw}\frac{\partial W}{\partial y} - 2\overline{w^2}\frac{\partial W}{\partial z}}_{\text{Shear Generation}} \underbrace{-2\frac{V}{r}\overline{w^2} - 2\frac{W}{r}\overline{vw} - 2\overline{w^2}\frac{\partial W}{\partial z}}_{\text{Curvature Generation}} \underbrace{+4\overline{vw}\Omega}_{\text{Coriolis Generation}} \tag{22}$$

$$P_{\overline{v^2}} = \underbrace{-2\overline{wv}\frac{\partial V}{\partial x} - 2\overline{v^2}\frac{\partial V}{\partial y} - 2\overline{vw}\frac{\partial V}{\partial z}}_{\text{Shear Generation}} \underbrace{+4\frac{W}{r}\overline{VW}}_{\text{Curvature Generation}} \underbrace{-4\overline{vw}\Omega}_{\text{Coriolis Generation}} \tag{23}$$

$$P_{\overline{vw}} = \underbrace{-\overline{uw}\frac{\partial V}{\partial x} - \overline{vw}\frac{\partial V}{\partial y} - \overline{w^2}\frac{\partial V}{\partial z} - \overline{uv}\frac{\partial W}{\partial x} - \overline{v^2}\frac{\partial W}{\partial y} - \overline{vw}\frac{\partial W}{\partial z}}_{\text{Shear Generation}} \underbrace{-\frac{V}{r}\overline{vw} + \frac{W}{r}\overline{u^2} - 2\frac{W}{r}(\overline{w^2}-\overline{v^2})}_{\text{Curvature Generation}} \underbrace{-2(\overline{w^2}-\overline{v^2})\Omega}_{\text{Coriolis Generation}} \tag{24}$$

where Ω is positive in the outward flow mode and negative in the inward flow mode.

The sum of curvature and Coriolis generation terms may be rewritten as follows.

$$P_{\overline{w^2}(curvature+coriolis)} = -2\frac{V}{r}\overline{w^2} - 2\frac{W}{r}\overline{vw}\left(1-2\frac{\Omega r}{W}\right) \tag{25}$$

$$P_{\overline{v^2}(curvature+coriolis)} = 4\frac{W}{r}\overline{vw}\left(1-\frac{\Omega r}{W}\right) \tag{26}$$

$$P_{\overline{vw}(curvature+coriolis)} = -\frac{V}{r}\overline{vw} + \frac{W}{r}\overline{u^2} + \frac{2W}{r}(\overline{w^2}-\overline{v^2})\left(1-\frac{\Omega r}{W}\right) \tag{27}$$

where $\frac{\Omega v}{W}$ is the local rotation number.

We see from the above equations that the magnitude and the sign of $\overline{vw}$, $\frac{\Omega v}{W}$ and $(\overline{w^2}-\overline{v^2})$ may be the parameters which primarily affect the turbulence structures in the rotating bend flow. If one considers the dynamic equation for the individual mean square turbulent velocities, a term $4\overline{vw}\Omega$ appears as a source (or sink depending on the sign of $\overline{vw}$) in the $\overline{w^2}$ Eq. (22), while a sink (source) of same magnitude appears in the $\overline{v^2}$ Eq. (23). The Coriolis generation term $-2(\overline{w^2}-\overline{v^2})\Omega$ in the $\overline{vw}$ equation can act as a sink or a source depending on the signs of $\overline{vw}$ and Ω. In the region of positive $\overline{vw}$, positive value of $-2(\overline{w^2}-\overline{v^2})\Omega$ acts as a source, while a sink in the region of negative $\overline{vw}$.

In the rotating straight channel flow, the Coriolis generation $-2(\overline{w^2}-\overline{v^2})\Omega$ in the $\overline{vw}$ equation decreases the positive level of $\overline{vw}$ near the suction surface, as shown in Fig. 11(d), so that it results in the decrease in the level of turbulent kinetic energy and mean square turbulent velocities in that region while generating opposite effects near the pressure surface. In Fig. 11(d), through the stations from $z=-3D_H$ to $\theta=22.5°$, we can find the decreases of $\overline{vw}$ level as with the rotation of bend. However, the decrease of $\overline{vw}$ level associated with bend rotation disappears as with the flow progress beyond $\theta=45°$. In the inlet tangent and the entrance region of the rotating bend of the square cross-section. we can clearly determined the effects of the Coriolis generation term in the $\overline{vw}$ equation on the level of turbulent kinetic energy. However, beyond $\theta=45°$, the effect of Coriolis generation term in $\overline{vw}$ the equation disappears gradually. The curvature of the bend augment the mean square radial turbulent velocities over the stream-wise turbulent velocity in some regions, reversing the sign of $-2(\overline{w^2}-\overline{v^2})\Omega$ in the $\overline{vw}$ equation. Therefore we cannot find the consistent trend in the variation of $\overline{vw}$ profiles beyond $\theta=45°$ in the rotating bend flow. As the flow progresses around the bend, the reduction of mean square turbulent velocities near the suction surface continues until the bend outlet. However, near the pressure surface, the level in the mean square turbulent velocities of the rotating bend flow falls below those of the stationary bend. In the inward flow mode, the Coriolis force is combined with the centrifugal force in a productive way in the outward radial direction to increase the secondary flow intensity. This increase in secondary flow intensity as shown in Figs. 8 (b) and 9(b) may advance the breakdown of a counter rotating secondary flow vortex into a multi-cellular pattern, preventing the increase of mean square turbulent velocities near the pressure surface of the stations beyond $\theta=45°$.

Comparisons of the measured mean stream-wise and radial velocity profiles of the rotating

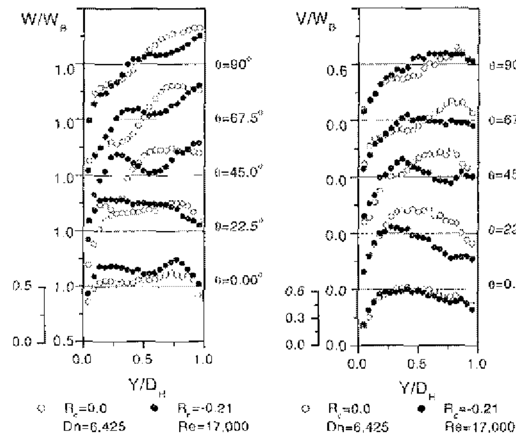

Fig. 12 Longitudinal variation of measured mean streamwise velocity (W/W_B) and mean radial velocity (V/W_BB) normalized by W_B along the center symmetry plane in the outward flow mode for higher Dean number and lower rotation number

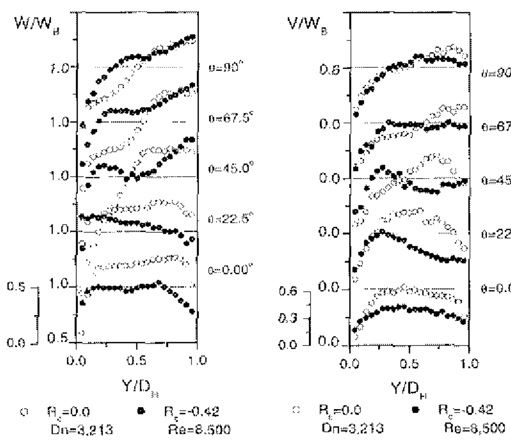

Fig. 13 Longitudinal variation of measured mean stream-wise velocity (W/W_B) and mean radial velocity (V/W_B) normalized by W_B along the center symmetry plane in the outward flow mode for lower Dean number and higher rotation number

and the stationary bend flows for the outward flow mode are shown in Figs. 12 and 13. In the outward flow mode, rotation of the bend damps the secondary flows in the entrance region of curved duct, and makes the mean stream-wise velocity profiles be flatter compared to the stationary bend flow due to the destructive combination of centrifugal and Coriolis forces. Comparing Figs. 12 and 13, we find that, with the decrease of rotation number in negative direction, W/W_B profile becomes flatter at the station beyond $\theta=45°$ while decreasing secondary flow intensity in the entrance region.

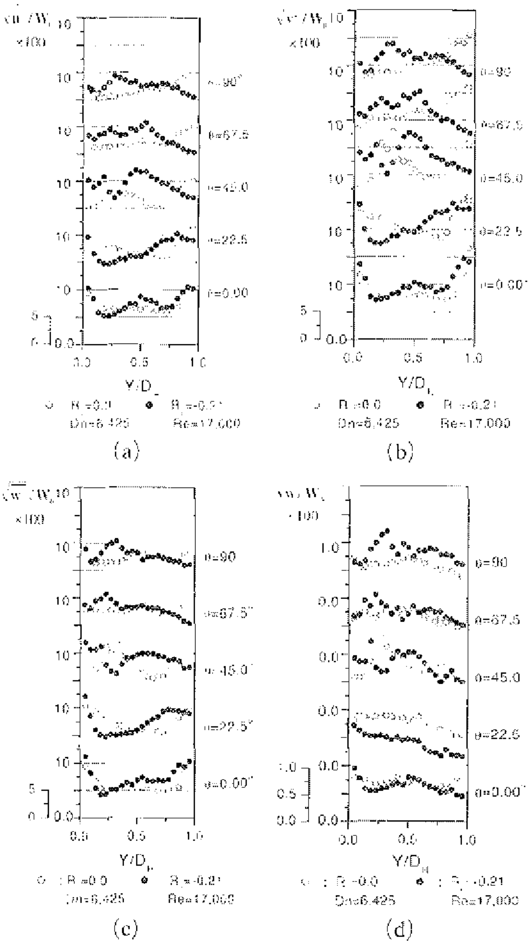

Fig. 14 Longitudinal variation of measured rms turbulent velocities ($\sqrt{\overline{u^2}}/W_B$, $\sqrt{\overline{v^2}}/W_B$, $\sqrt{\overline{w^2}}/W_B$) and Reynolds shear stress ($\overline{vw}/W_B^2$) normalized by W_B and W_B^2 in the outward flow mode for lower Dean and rotation numbers

Longitudinal variations of $\sqrt{\overline{u^2}}/W_B$, $\sqrt{\overline{v^2}}/W_B$ and $\sqrt{\overline{w^2}}/W_B$ for the outward flow mode contained in Fig. 14 show the opposite trends of the variations of inward flow mode shown in Fig. 11. In the entrance region of bend, the radial and the stream-wise rms turbulent velocities normalized by W_B decrease in the inner wall side while increase in the outer wall side. But the opposite trend, which is more obviously found in the radial rms turbulent velocity profiles, occurs as with the flow progress beyond $\theta=45°$. Opposite signs of the curvature and Coriolis generation terms, $\overline{vw}W/r$ and $4\Omega vw$, in the $\overline{v^2}$ and $\overline{w^2}$ equations may cause these differences in the variations of $\overline{v^2}$ and $\overline{w^2}$ profiles near the suction surface. In the entrance region, the levels of $\sqrt{\overline{v^2}}/W_B$ near the wall side are larger than those of the core region. But beyond $\theta=45°$ the level of $\sqrt{\overline{v^2}}/W_B$ of the core region becomes larger than those of near wall sides. This is due to the change of sign in the Coriolis generation term $-2(\overline{w^2}-\overline{v^2})\Omega$ in the $\overline{vw}$ equation as $\overline{v^2}$ increases over the $\overline{w^2}$ as shown in Fig. 14. The reversal of the sign of Coriolis generation term $-2(\overline{w^2}-\overline{v^2})\Omega$ in the $\overline{vw}$ equation may induce the obvious decrease in the level of $\overline{vw}/W_B$, at the station $\theta=22.5°$ in Fig. 14(d).

4. Conclusions

Hot-wire measurement of the mean and turbulent velocities in rotating 90-degree bend flows of a square cross-section are reported and the effects of Coriolis and centrifugal forces on the mean motion and the turbulent structures are explored. From the investigation of longitudinal variations of the mean stream-wise and the radial velocities, the Reynolds stresses, and the pressure coefficients, the following conclusions are drawn.

(1) The productive merging of the Coriolis force and the centrifugal force due to the bend curvature in the outward radial direction increase the secondary flow intensity in the entrance re-

gion of the bend. However, beyond 45 degree position of the bend, the centrifugal force due to bend rotation may promote the break down of the counter rotating vortex pair into multi-cellular pattern, thereby decreasing the generation rate of turbulent kinetic energy.

(2) The Coriolis generation term in the $\overline{vw}$ equation may decrease both the Reynolds stresses and turbulent the kinetic energy near the suction surface while keeping intact those of the near pressure surface due to the advanced break down of counter-rotating vortex pairs into multi-cellular patterns in that region.

(3) In the outward flow mode, the effects of Coriolis generation terms in the $\overline{vw}$ equation on the level of turbulent kinetic energy are more visible in the entrance region due to the decrease in secondary flow intensity caused by the destructive addition of the Coriolis and the centrifugal forces.

References

Anderson, H. I. and Kristoffersen, R., 1995, "Turbulent Statistics of Rotating Channel Flow," *Turbulent Shear Flow*, Vol. 9, Springer, Berlin, pp. 53~70.

Bo, T., Iacovides, H. and Launder, B. E., 1995, "Developing Buoyancy-Modified Turbulent Flow in Ducts Rotating in Orthogonal Mode," *Trans. ASME, J. of Turbomachinery*, Vol. 117, pp. 65~95.

Champagne, F. H., Sleicher, C. A. and Wehrmann, O. H., 1967, "Turbulence Measurements with Inclined Hot-Wire," *J. Fluid Mech.*, Vol. 28, part 1, pp. 153~175.

Choi, Y. D., Shin, J. K., Chun, K. H. and Humphrey, J. A. C., 1997, "Modeling Turbulent Flow in a Curved Duct of Square Cross-Section," *Proc. of 11^th^ Symposium on Turbulent Shear Flows*, Grenoble, France, pp. 3.47~3.52.

Choi, Y. D., Moon, C. and Yang, S. H., 1990, " Measurement of Turbulent Flow Characteristics of Square Duct with a 180Degree Bend by Hot-Wire Anemometer," *Proc. of the International Symposium on Turbulence Modeling and Experiments*, Dubrovnik, pp. 429~438.

Jackson, T. W. and Lilly, D. G., 1983, "Single Wire Swirl Flow Turbulence Measurement," *AIAA 83-1202*, Cleveland, Ohio.

Janjua, S. I., Mclaug, D. K., Jackson, T. W. and Lilly, D. G., 1982, "Turbulence Measurements in a Confined Jet Using a Six-Orientation Hot-Wire Probe Technique," *AIAA 82-1262*, Cleveland, Ohio.

Johnston, J. P., Halleen, R. M. and Lezius, D. K., 1972, "Effects of Spanwise Rotation on the Structure of Two-Dimensional Fully Developed Turbulent Channel Flow," *J. Fluid Mech.*, Vol. 56. No. 3, pp. 533~557.

Kajishima, T., Miyake, Y. and Nishimoto, 1991, "Large Eddy Simulation of Turbulent Flow in a Square Duct," *Trans. JSME (B)*, 57-540, pp. 2530~2537.

Kim, J., 1983, "The Effect of Rotation on the Turbulent Structure," *Proc. of 4th International Symposium on Turbulent Shear Flows*, Karlsruhe, pp. 6~14.

King, C. F., 1978, Ph.D. Thesis, Univ. College of Wales, Cardiff, Wales.

Kristofferson, R. and Andersson, H. I., 1993, "Direct Numerical Simulations of Low Reynolds Number Turbulent Flow in a Rotating Channel," *J. Fluid Mech.*, Vol. 256, pp. 163~197.

Kristofferson, R., Nilsen, P. J. and Andersson, H. I., 1990, "Validation of Reynolds Stress Closures for Rotating Channel Flows by Means of Direct Numerical Simulations," *Proc. International Symposium on Engineering Turbulence Modeling and Measurements*, Dubrovinik, pp. 55~64.

Koyama, D. K. and Ohuchi, M., 1985, *Proc. of 5th International Symposium of Turbulent Shear Flows*, Cornell, pp. 21~19.

Launder, B. E., Tselepidalsis, D. P. and Younis, B. A., 1987, "A Second-Moment Closure Study of Rotating Channel Flow," *J. Fluid Mech.*, Vol. 183, pp. 63~75.

Launder, B. E. and Tselepidalsis, D. P., 1994, "Application of a New Second Moment Closure to Turbulent Channel Flow Rotating in Orthogonal Mode," *International Journal of Heat and Fluid Flow*, Vol. 15, No. 1, pp. 2~10.

Morris, W. D., 1981, "Heat Transfer and Fluid

Flow in Rotating Coolant Channels," *Chichester : John Wiley and Sons.*

Murata, A. and Mochizuki, S., 1999, "Effect of Cross-Sectional Aspect Ratio on Turbulent Heat Transfer in an Orthogonally Rotating Rectangular Smooth Duct," *International J. of Heat and Mass Transfer*, Vol. 42, pp. 3803~3814.

Pattersson, B. A. and Anderson, H. I., 1997, "Near-Wall Reynolds-Stress Modeling in Non-inertial Frames of Reference," *Fluid Dynamics Res.*, Vol. 19, pp. 251~276.

Tafti, D. K. and Vanka, S. P., 1991, "A Numerical Study of the Effect of Span-wise Rotation on Turbulent Cannel Flow," *Phys. Fluids A*, Vol. 3, No. 4, pp. 642~656.

Younis, B. A., 1993, "Prediction of Turbulent Flows in Rotating Rectangular Ducts," *Trans. ASME, J. of Fluids Eng.*, Vol. 115, pp. 646~652.